ORIGINAL PAPER

Interleukin-8 release by endothelial colony-forming cells isolated from idiopathic pulmonary fibrosis patients might contribute to their pathogenicity

Adeline Blandinières[1,2,3] · Nicolas Gendron[1,2,3] · Nour Bacha[2,3] · Ivan Bièche[2,4] · Richard Chocron[2,5,6] · Hilario Nunes[7] · Nathalie Nevo[2,3] · Elisa Rossi[2,3] · Bruno Crestani[8] · Séverine Lecourt[2,3] · Sylvie Chevret[9] · Anna Lokajczyk[2,3] · Virginie Mignon[2,10] · Alexandre Kisaoglu[3] · Karine Juvin[11] · Sebastien Bertil[1] · Dominique Valeyre[7] · Audrey Cras[2,3,12] · Pascale Gaussem[1,2,3] · Dominique Israël-Biet[2,3,11] · David M. Smadja[1,2,3]

Abstract

Introduction Idiopathic pulmonary fibrosis (IPF) is a devastating disease characterized by obliteration of alveolar architecture, resulting in declining lung function and ultimately death. Pathogenic mechanisms involve a concomitant accumulation of scar tissue together with myofibroblasts activation and a strong abnormal vascular remodeling. Endothelial progenitor cells (ECFC subtype) have been investigated in several human lung diseases as a potential actor in IPF. We previously demonstrated that ECFCs are down-regulated in IPF in contrast to healthy controls. We postulated here that ECFCs might behave as a liquid biopsy in IPF patients and that they exert modified vasculogenic properties.

Methods and results ECFCs isolated from controls and IPF patients expressed markers of the endothelial lineage and did not differ concerning adhesion, migration, and differentiation in vitro and in vivo. However, senescent and apoptotic states were increased in ECFCs from IPF patients as shown by galactosidase staining, p16 expression, and annexin-V staining. Furthermore, conditioned medium of IPF-ECFCs had increased level of interleukin-8 that induced migration of neutrophils in vitro and in vivo. In addition, an infiltration by neutrophils was shown in IPF lung biopsies and we found in a prospective clinical study that a high level of neutrophils in peripheral blood of IPF patients was associated to a poor prognosis.

Conclusion To conclude, our study shows that IPF patients have a senescent ECFC phenotype associated with an increased IL-8 secretion potential that might contribute to lung neutrophils invasion during IPF.

Keywords Endothelial progenitor cells · Endothelial colony-forming cells · Liquid biopsy · Interleukin-8 · Idiopathic pulmonary fibrosis

✉ David M. Smadja
david.smadja@aphp.fr

1 Hematology Department, AP-HP, European Georges Pompidou Hospital, 20 rue Leblanc, 75015 Paris, France

2 Paris Descartes University, Sorbonne Paris Cité, Paris, France

3 Inserm UMR-S1140, Paris, France

4 Pharmacogenomics Unit, Department of Genetics, Institut Curie, Paris, France

5 Emergency Medicine Department, AP-HP, European Georges Pompidou Hospital, Paris, France

6 Inserm UMR-S970, PARCC, Paris, France

7 Avicenne Hospital, Respiratory Medicine Department, AP-HP, Paris, France

8 Bichat Hospital, Respiratory Medicine Department, AP-HP, Paris, France

9 Biostatistics Unit, AP-HP, Saint Louis Hospital, Paris Diderot University, Paris, France

10 Cellular and Molecular Imaging Facility, Faculty of Pharmacy of Paris, Inserm US 25, CNRS UMS 3612, Paris Descartes University, Paris, France

11 Respiratory Medicine Department, AP-HP, European Georges Pompidou Hospital, Paris, France

12 Cell Therapy Departement, AP-HP, Saint Louis Hospital, Paris, France

Introduction

Idiopathic pulmonary fibrosis (IPF) is a progressive and lethal disease [1] characterized by damage to the lung parenchyma with excess matrix deposition. Its prognosis is poor with a median survival of 2–4 years after diagnosis [1]. The chronic progressive decline in lung function appears to result from persistent non-resolving injury of the epithelium, impaired restitution of the epithelial barrier in the lung, and enhanced fibroblast proliferation. IPF is therefore a disease primarily of epithelial cell dysfunction in a context of multiple genetic and environmental risk factors [2]. The pathogenic pathways involved in the local fibrogenesis are still elusive. Next to the epithelium, pulmonary endothelial cells might play a role in IPF pathogenesis through several mechanisms including the endothelial-mesenchymal transition [3] and, as recently confirmed in a bleomycin murine model of pulmonary fibrosis [4], through modified functional capacities. It is noticeable that in the IPF lung parenchymal lesions are constantly associated to a major vascular remodeling process associating a rarefaction of vessels in fibrotic areas and their aberrant proliferation in border of these areas [5]. It is associated with an imbalance between markers of endothelial activation and regeneration [6]. Mechanisms underlying this vascular remodeling are still to elucidate. One of the hypotheses could be the deregulation of angiogenic and angiostatic factors that we and others have previously shown [7, 8].

Endothelial progenitor cells (EPCs) are now well established as postnatal vasculogenic cells in humans [9]. It is now admitted that endothelial colony-forming cells (ECFCs or blood outgrowth endothelial cells, BOECs) [9] are the vasculogenic subtype. ECFCs are progenitor cells committed to endothelial lineage and have strong vasculogenic properties in preclinical models of vascularization [9]. They express specific endothelial lineage markers [10] and originate from bone marrow [9] although some organs, and particularly the lung, can serve as a cellular reservoir for ECFCs [9, 11]. Circulating ECFCs can be considered as a potential liquid biopsy in several pulmonary-associated vascular disorders, due to their altered functions such as found during pulmonary arterial hypertension with BMPRII mutation [12], bronchopulmonary dysplasia [13], or chronic obstructive pulmonary disease [14]. We and others have described decreased numbers of EPCs and/or ECFCs in IPF [6, 15]. In addition, these cells have the ability to adopt a fibroblastic phenotype through an endothelial-mesenchymal transition mechanism (TEndoM) [16]. Suspected to play a role in IPF pathogenesis, ECFCs have, however, never been characterized so far in this context in terms of phenotypic and functional properties.

The purpose of this study was to investigate whether ECFCs are dysfunctional in IPF, and to progress in the understanding of their potential contribution to the development of lung fibrosis or to angiogenic disorders observed in IPF.

Material and methods

Study population

A French prospective and multicentric cohort of IPF (COFI) was started in 2008 (registry number 2006-108). Inclusion criteria comprised the diagnosis of IPF, dating back to less than 9 months, based upon either surgical biopsy or a characteristic computerized tomography (CT) scan pattern of usual interstitial pneumonia according to the ATS/ERS consensus [17]. All demographic, comorbidities, clinical and functional data were prospectively and serially recorded. All complications of the disease (acute and subacute exacerbations, progression, development of pulmonary hypertension, hospitalizations, death) as well as lung transplantation were notified during follow-up. Three teaching hospitals in the Ile-de-France area participated to study of the circulating endothelial compartment in these patients, specifically approved by the Ethics committee of Ile-de-France II (registry number 2006-108). Their leukocyte subpopulations were also serially assessed. To this purpose, blood samples were collected at inclusion into the cohort from 65 subjects. Their demographic and clinical characteristics are shown in Supplemental Table 1. Leukocyte, neutrophil, lymphocyte, monocyte, and platelet counts were measured using a LH-750 (Beckman Coulter, USA) and $CD34^+CD45^{dim}$ populations corresponding to hematopoietic stem cells were measured using the StemKit reagents (IM3630, Beckman Coulter, USA).

Cells isolation and culture

Human umbilical cord bloods were obtained from the Cell therapy Unit of Saint-Louis Hospital (AP-HP, Paris). Cord-blood endothelial colony-forming cells (CB-ECFCs) were isolated from the adherent mononuclear cell (MNC) fraction as previously described [10]. ECFCs isolated from IPF patients (IPF-ECFCs) and PB-ECFCs from control adult samples were isolated as previously described [18, 19]. ECFCs were then expended on fibronectin (FN)-coated plates (Merck, Germany) using EGM-2MV (Lonza, USA) supplemented with 10% fetal bovine serum (FBS) and used between passages 3 to 6. Mesenchymal stromal cells (MSC) were isolated from the MNC fraction of healthy donor human adult bone marrow, as previously described [20] and cultivated in α-MEM medium containing GlutaMAX™

(Gibco, USA) supplemented with 10% FBS and 1 ng/mL bFGF (R&D Systems, USA).

IPF-ECFC phenotype was compared to PB-ECFCs as well as to CB-ECFCs and MSCs considered, respectively, as references of endothelial and mesenchymal phenotypes.

Characterization of IPF-ECFCs by RT-qPCR

ECFCs in culture were lysed in RNable (Eurobio, France). RNA was extracted with chloroform and precipitated with isopropanol before reverse transcription in cDNA using the Quantitect Reverse Transcription kit (Qiagen, Germany) according to the manufacturer's instructions. Quantitative PCR was performed as previously described [10]. As an endogenous RNA control, we quantified transcripts of human *GAPDH* (4326317E, Life Technologies, USA). Probes for transcripts of interest were *KDR* (Hs00911705_g1, Life Technologies, USA), *CDH5* (Hs00901465_m1, Life Technologies, USA), *THY1* (Hs00264236_s1, Life Technologies, USA), CXCR1 (Hs01921207_s1, Life Technologies, USA), and CXCR2 (Hs01891184_s1, Life Technologies, USA). Data were analyzed with the SDS v2.3 software and are expressed as "normalized mRNA level" as described elsewhere [21].

For quantification of *CDKN1A, CDKN2A*, and *TP53*, real-time polymerase chain reaction was performed as previously described [21]. Primers sequences are shown in Supplemental Table 2. Transcripts of *TBP* gene, encoding the TATA box-binding protein, were used as endogenous control.

Flow cytometry immunophenotyping

Cultured cell were detached with trypsin, washed in PBS containing 10% FBS, and resuspended in 100 μL of PBS/1% BSA. Cells were labeled with APC-Cy7 conjugated mouse anti-human CD31 IgG1 (WN59, Biolegend, USA), FITC conjugated mouse anti-human CD45 IgG1 (IM0 782U, Beckman Coulter, USA), PE conjugated mouse anti-human CD90 IgG1 (IM18400U, Beckman Coulter, USA), PE conjugated anti-CXCR1 (FAB330P, R&D, USA), or PE conjugated anti-CXCR2 (FAB331P, R&D, USA) at 1/20 dilution for 30 min on ice away from light. Isotype-matched anti-mouse IgG1 from the same manufacturer were used as negative control. Acquisition of 30,000 events was performed on Attune acoustic flow Cytometer (Life Technologies, USA) and analyzed on Attune cytometer software (Life Technologies, USA). Results are expressed as median of fluorescence.

Adhesion assay

ECFCs were previously stained with CFSE (CellTrackerTM, Life Technologies, USA) and then plated at a density of 7.10^4 cells/well in EGM-2MV 10% FBS on MillicellsEZ slides of 4 wells (Merck Millipore, Germany) previously coated with collagen, fibronectin, or seeded with confluents MSC. After 30 min at 37 °C, wells were washed with PBS to retire non-adherent cells and adherent cells were fixed with methanol. For each well, 5 images (×10) were taken with epifluorescence microscope (Zeiss Observer D1, Histolab software) and adherent cells were counted with Image J software.

Wound healing assay

In vitro wound healing assay was performed using culture inserts (IBIDI, Germany). ECFCs were seeded at 10^4 cells/well in EGM-2MV 10%FBS (70 μL per well). When confluence was reached, culture inserts were removed creating a reproducible "wound." Photographs were taken at 0, 1, 4, 8, 18, and 24 h after removal of inserts. These photographs were analyzed with Image J software: the area of injury at each time was measured in order to calculate a percentage of injury repair with respect to the area of initial wound.

Chemotactic migration assay

24-well Transwell PET membranes with 8-μm-diameter pores (Corning, USA) were coated with 0.2% gelatin at 37 °C for 30 min. Then, 1.5×10^4 ECFCs/well were loaded in EBM-2 0.5% FBS into the upper part of the chamber. The lower part of the chamber was filled with EGM-2MV medium. Migration was allowed for 5 h at 37 °C. Membranes were then fixed in 4%PFA and cells present on the upper face of the membrane were removed by wiping with a cotton bud. Mounting was achieved with Vectashield mounting medium containing DAPI (H-1200, Vector Labs, USA) and membranes were photographed with an epifluorescence microscope (magnification ×20, Evos XL, Life technologies, USA). For each membrane, numbers of cells present on ten separate fields were counted with Image J software.

In vitro capillary-like growth assay

Matrigel™ Matrix Growth Factor Reduced (BD Biosciences, USA) was deposed at 4 °C in 48-well plates (200 μL/well) on crushed ice. Polymerization of the gel was achieved by incubating the plate at 37 °C for 1 h. 5.10^4 cells/well were added in 500 μL of EGM-2MV medium supplemented with 10% FBS. Formation of pseudo-tubes was observed after 1, 4, 8, 18, and 24 h incubation at 37 °C and images were taken with an inverted microscope with phase contrast mode. Quantification of the total length of pseudo-tubes formed at 8 h and 24 h was performed with the macro Angiogenesis

Analyzer on Image J (http://image.bio.methods.free.fr/Image J/?Angiogenesis-Analyzer-for-ImageJ).

3D sprouting assay

Three-dimensional fibrin gel assays were performed as previously described [22]. ECFCs were seeded on Cytodex-3 beads (Sigma-Aldrich, Germany) and then embedded in 2.5 mg/mL fibrin gel at the concentration of 250 beads/well in 4-well Lab-TekII (Nunc, USA). MSCs were plated on top of the gel (80,000 cells/well) in EGM-2MV medium. After 7 days of culture, MSCs were trypsinized and gels fixed with 4% PFA. Gels were stained with Alexa Fluor-488-conjugated phalloidin (Thermo Fischer Scientific, USA) and TO-PRO-3 (Thermo Fischer Scientific, USA). Images were acquired by confocal microscopy (Leica Confocal laser scanning microscope TCS SP8 and Leica Las X Lite software). Number of sprouts and cumulative tube length per bead were measured using Fiji Macro as previously described [23].

In vivo matrigel implant assay

All animal experiments were performed at the Animals facility of the faculty of Pharmacy of Paris Descartes University and approved by the ethic comity Paris V (project no. 201610201540639). For Matrigel™ implant assay, 1.5×10^6 ECFCs and 1.5×10^6 MSCs were resuspended in 200 μL of Matrigel™ (BD Matrigel™Matrix, BD Biosciences, USA) and injected subcutaneously in the back of NMRI-Fox1[nu]/1[nu] MALE mice (Janvier Laboratories, France). Manipulation of Matrigel before injection was done on ice to prevent from early polymerization. Implants were removed after 10 days under anesthesia by a mix oxygen-isoflurane 2%. Implants were fixed in 4% PFA and embedded in paraffin. Slides were stained with hematoxylin and eosin (Olivia Bawa, Laboratoire de Pathologie Expérimentale, Institut Gustave Roussy, France). For each implant, three non-contiguous sections were analyzed by counting functional vessels containing red blood cells on five images for each section (×40). For the neutrophil recruitment implant assay, conditioned media (CM) were 40-fold concentrated with Amicon-3k devices (Merck Millipore, USA). 50 μL of concentrated CM was mixed with 200 μL of Matrigel™ (BD Matrigel™Matrix, BD Biosciences, USA) and injected subcutaneously in the back of male NMRI-Fox1[nu]/1[nu] mice (Janvier Laboratories, France). In indicated experiments, antibody against CXCL-8 (AF-208-NA, R&D Systems, USA) or its corresponding isotype (10 μg/implant) was added to concentrated CM. After 2 days, implants were explanted, fixed with 4% PFA, and embedded in paraffin. Infiltration by neutrophils was evaluated after MPO staining (dilution 1/200e, ab9535, Abcam, United Kingdom) and counterstained with Bluing

Reagent performed on a BenchMark ULTRA system (Ventana, USA). For each implant, three non-contiguous sections were analyzed: area of infiltrated surface was quantified with Image J software and normalized to the perimeter of the corresponding section.

Soluble factors secreted by ECFCs

Cells in culture were growth for 48 h in EBM-2 supplemented with 0.5% FBS. Conditioned medium (CM) was harvested, centrifuged twice (at 405 g for 5 min then at 16,435g for 2 min), and stored at -80 °C. Simultaneously, cells were numbered. Concentrations of VEGF-A (BMS80277F), FGF-2 (BMS82074FF), sVEGFR-1 (BMS80268FF), sVEGFR-2 (BMS82019FF), G-CSF (BMS82001FF), HGF (BMS8269FF), MIP-1α (BMS8229FF), MIP-1β (BMS82030FF), IL-8 (BMS8204FF), MCP-1 (BMS8281FF), t-PA (BMS8258FF), PAI-1 (BMS82033FF) were determined with Flowcytomix Simplex Kit (eBioscience, USA) according to manufacturer's instructions. Briefly, conditioned media was incubated with fluorescent beads coupled with a panel of antibodies, each one being specific for a factor. Hybridization of a second antibody coupled with biotin allowed to quantify precisely the amount of soluble factor after addition of streptavidin–phycoerythrin. Analysis was realized with Flowcytomix Pro Software.

IL-8, IL-6, TNF-α, and TGF-β1 were quantified with Quantikine ELISA kits (R&D Systems, USA) according to manufacturer's instructions. All results were expressed in ng/10^6 cells.

Cell proliferation assays

To evaluate proliferation potential, bromodeoxyuridine (BrdU, reference B5002, Sigma-Aldrich, Germany) was added to cells in culture (30 μM) and incubated for 15 min at 37 °C. Cells were then detached with trypsin and fixed with ethanol 100% for 30 min at 4 °C. After acid lysis (HCl 2M), cells were resuspended in a buffer containing normal goat serum (1/200e, X907 Dako, Denmark), Tween 20 (1/200e, P2287, Sigma-Aldrich, Germany), and Hepes (1/50e, 15630-056, Invitrogen USA) in PBS. Incorporation of BrDU was detected with anti-BrDU antibody (1/25e, MAS250B, Seralab, Interchim, France) and secondary antibody Goat Anti-Rat IgG FITC (20 μg/mL, 3030.2, product Southern Biotechnologie, Cliniscience, France). DNA amount was evaluated by incorporation of propidium iodure (25 μg/mL, 28707-5, Sigma-Aldrich, Germany). Acquisition was performed on Attune cytometer (Life technologies, USA).

Senescence assay

ECFCs were seeded in triplicate in 24-well plates at a density of 10,000 cells/cm^2. Senescence was quantified with colorimetric detection of senescence-associated ß-galactosidase (SA-β-gal) using a Senescence Detection Kit (Promocell, Germany) according to the manufacturer's instructions. S-β-gal-positive cells were counted in nine randomly selected microscopic fields (objective ×20). Results were expressed in percentage of total cells.

Apoptosis assay

Apoptosis was quantified with Annexin V/7-AAD kit (Beckman Coulter, USA) according to manufacturer's instructions on Attune cytometer (Life technologies, USA). Results were expressed as a percentage of viable cells (Annexin V − 7 AAD −), early apoptosis cells (Annexin V + 7 AAD −), late apoptosis cells (Annexin V + 7 AAD +), dead cells (Annexin V − 7 AAD +).

IL-8 quantification by ELISA in plasma samples

IL-8 concentration in 50 plasma samples of IPF patients included the COFI cohort described above and 10 of control healthy patients as previously described [24] were determined with Quantikine HS Elisa kit (R&D Systems, USA) according to manufacturer's instructions.

Neutrophil migration assay

Blood samples collected on EDTA were obtained from healthy volunteers from Etablissement Français du Sang (EFS, convention n° 13/EFS/64). Neutrophils (PMNs) were isolated with MACSxpress Neutrophil Isolation Kit (Miltenyi Biotech, Germany) according to manufacturer's instruction. 24-well Transwell PET membranes with 3 μm pore diameter (Corning, USA) were blocked with EBM-2 0.5% FBS at 37 °C for 30 min. Then, 1×10^5 PMNs/well were loaded in EBM-2 into the upper part of the chamber. The lower part of the chamber was filled with conditioned media. For indicated experiments, CXCL8 antibody (AF-208-NA, R&D Systems, USA) was added at a 5 μg/mL concentration. Migration was allowed for 90 min at 37 °C. Then, medium in the lower part of the chamber was collected and neutrophils were counted with flow cytometry (Accuri, Beckton Dickinson, USA).

This Ab has also been used in immunoanalysis of IL-8 expression in lungs (Supplementary Fig. 1).

Neutrophil staining on human lung biopsies

Human IPF lung specimens were recovered after surgical biopsies performed for diagnosis purposes ($n = 6$). Three-mm-thick paraffin-embedded sections were stained with hematoxylin and eosin to evaluate parenchyma and vessel morphology. Tissues obtained after lung resection for a localized tumor served as controls.

Lung tissue neutrophil density was evaluated after MPO staining (dilution 1/200e, ab9535, Abcam, United Kingdom) and counterstained with Bluing Reagent performed on a BenchMark ULTRA system (Ventana, USA). For each biopsy, 6 fields were photographed (objective x40) and neutrophils were counted with Image J software. Results are expressed as a number of neutrophils /mm^2.

Statistics

All analyses were performed with Prism software 5 (Graph-Pad). Results were analyzed with non-parametric test of Mann–Whitney or Kruskal–Wallis test followed by Dunn multiple comparisons post-test if there were more than two groups. p value < 0.05 was considered as statistically significant. Aberrant values were identified with Dixon test and excluded from analysis. Kendall rank correlation test was used to analyze the association between IL-8 plasma levels and the white blood cells and neutrophils.

Results

Phenotypic characterization of IPF-ECFCs

IPF-ECFCs as well as PB-ECFCs were positive for CD31 and negative for CD45 and CD90 by flow cytometry analysis, consistent with the current literature (Fig. 1a). No difference in median of fluorescence intensity ([min–max]) was noticed between the two populations (IPF-ECFC vs PB-ECFC: CD31 44,448 [22,632–77,614] vs 32,282 [20,810–43,754], CD45 46 [0-175] vs 4 [0–8], CD90 15 [0–92] vs 3 [4–15]). Endothelial and mesenchymal marker gene expression was further quantified by RT-qPCR. IPF-ECFC and PB-ECFCs expressed endothelial markers *CDH*5 (VE-cadherin) and *KDR* (VEGFR-2) similarly to CB-ECFCs. However, *THY1* (mesenchymal marker CD90) was only expressed in MSCs (Fig. 1b).

IPF-ECFCs have vasculogenic properties comparable to controls

To date, several reports have shown decreased numbers of EPCs and/or ECFCs in IPF patients but no data are available concerning their vasculogenic properties. We evaluated

A

IPF-ECFC

PB-ECFC

B
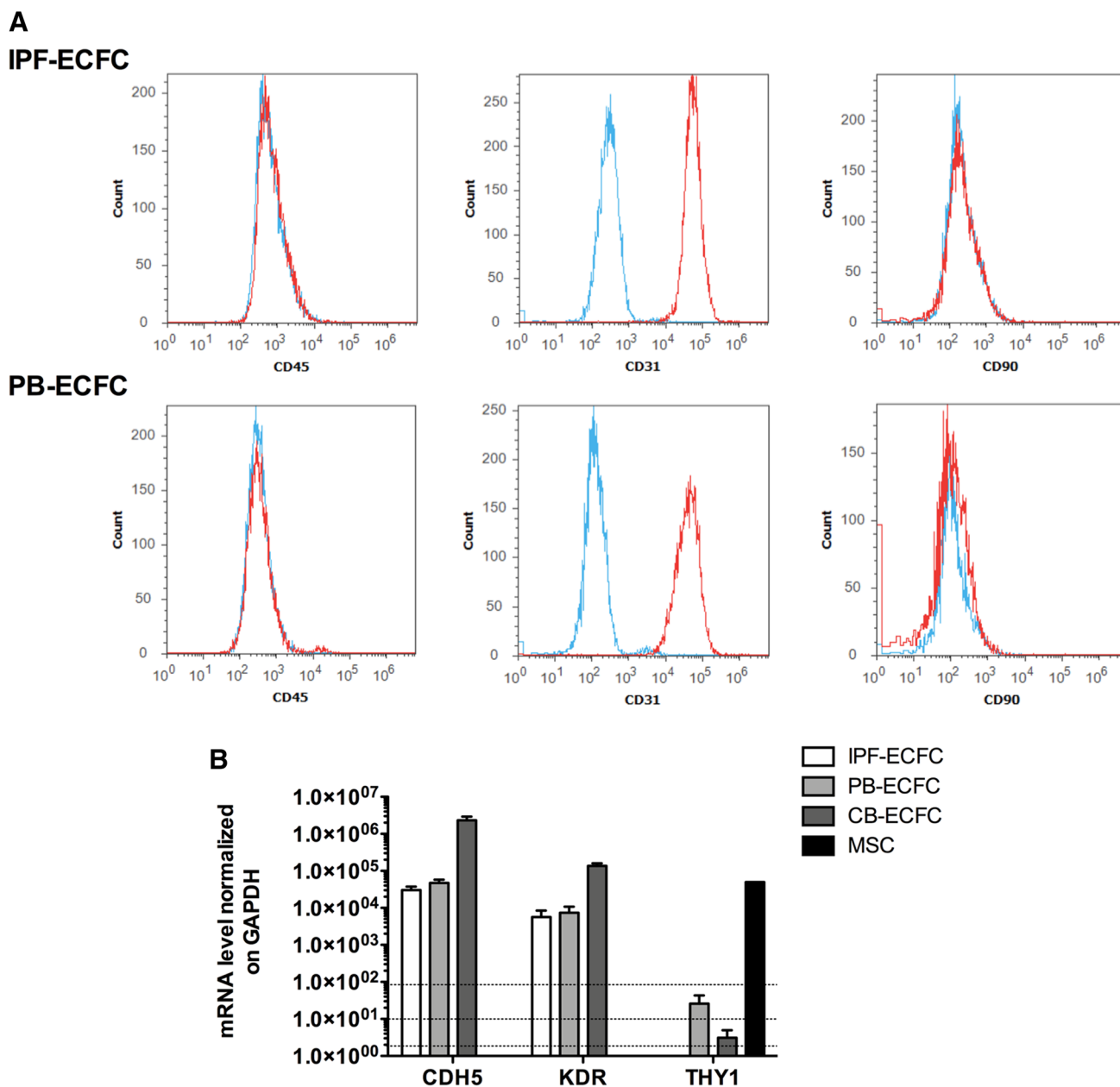
Fig. 1 Characterization of IPF-ECFCs compared to PB-ECFCs, CB-ECFCs or MSCs. **a** Typical experiment showing expression of CD45, CD31 or CD90 evaluated by cytometry (red curve: specific mAb, blue curve: control isotype). **b** Quantitative expression of CDH5, KDR, and THY-1 genes measured by RT-qPCR ($n=3$)

adhesion, migration, and differentiation capacities of IPF-ECFCs in comparison to PB-ECFC controls.

Adhesion properties of IPF-ECFCs on several supports (plastic, fibronectin, collagen, MSCs) were assessed. No significant difference was observed irrespective of the support used ($p = 0.49$; 0.07; 0.96 and 0.27 for plastic, fibronectin, collagen, and MSCs, respectively) (Fig. 2a). Migration properties of IPF-ECFCs were studied using two models: wound healing assay and Transwell® assay. In both models, IPF-ECFC migration properties were similar

to those of PB-ECFCs ($p = 0.82$ and 0.39, respectively) (Fig. 2b, c). Finally, IPF-ECFC differentiation capacities were evaluated by vessel formation in a Matrigel™ model in vitro and in vivo. In vitro, IPF-ECFCs were able to form pseudo-tubes similarly to PB-ECFCs and there was no significant difference between the two populations in terms of total length of formed tubes at 8 h or 24 h ($p = 0.73$ and 0.11, respectively) (Fig. 3a). In vivo, IPF-ECFCs were again comparable to PB-ECFCs, forming similar numbers of functional vessels properly connected to the mouse
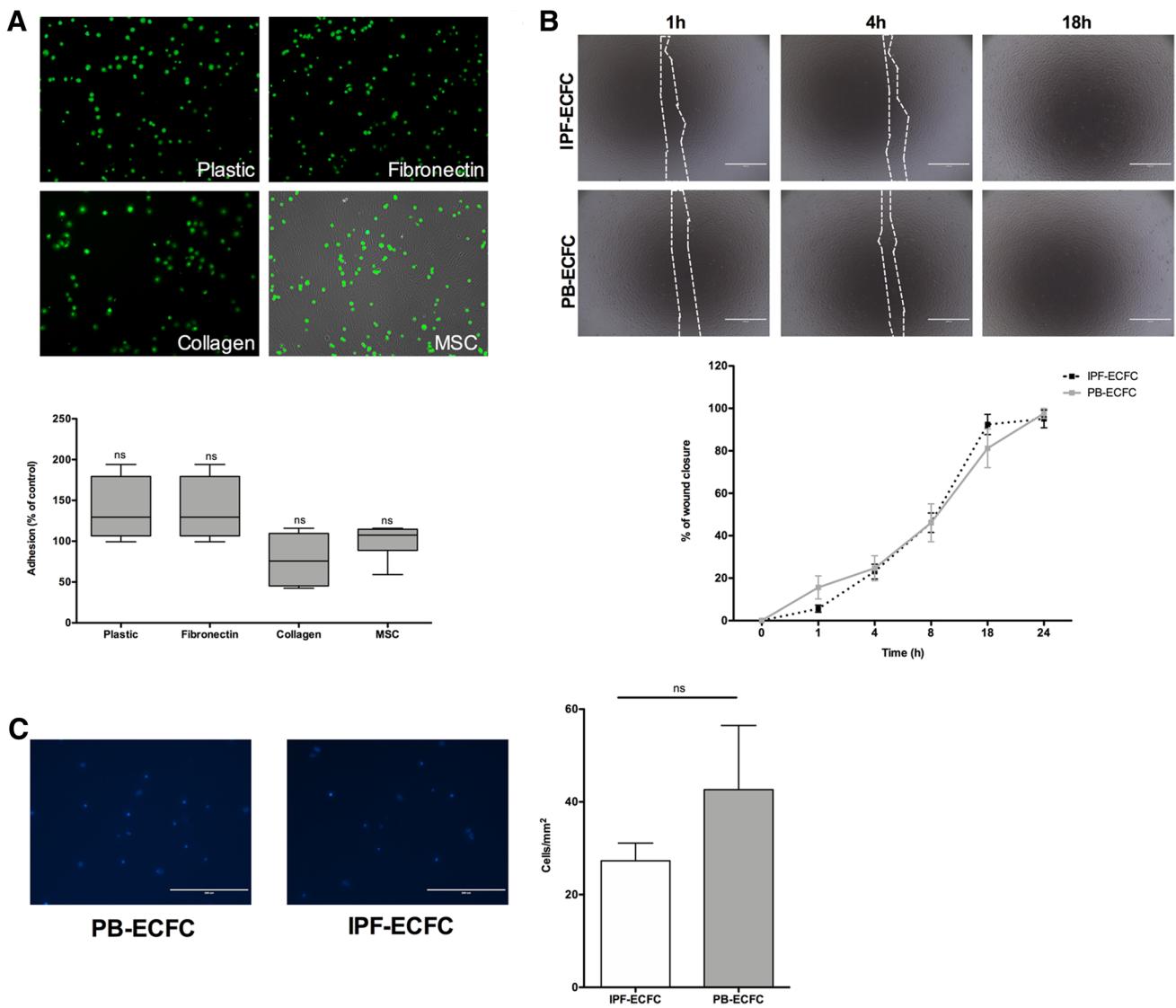
Fig. 2 Vasculogenic properties of IPF-ECFCs compared to PB-ECFCs. **a** Adhesion of IPF-ECFCs on plastic, fibronectin, collagen, or MSCs (ECFCs stained with CFSE, magnification ×10), quantification of adhesion (% of control) ($n = 5$–6). **b** Wound healing assay, images taken at 1 h, 4 h, 8 h, 18 h or 24 h (scale 1000 μm), % of wound closure ($n = 7$). **c** Chemotactic migration assay (ECFCs stained with DAPI, scale 200 μm), number of migrated cells/mm^2 ($n = 3$–5). ns $p > 0.05$

vascular system and filled with red blood cells ($p = 0.64$) (Fig. 3b). These results were further completed by a 3D sprouting assay where PB-ECFCs are known to form very few sprouts compared to CB-ECFCs [25]. Again, no significant difference was observed in this assay between IPF-ECFCs and PB-ECFCs in terms of sprout numbers or length ($p = 0.63$ and 0.40, respectively) (Fig. 3c).

IPF-ECFCs exhibit increased senescence markers compared to controls

Senescence was assessed in culture by ß-galactosidase staining of ECFCs aged 30 or 45 days. At 30 days, ß-galactosidase positivity was significantly higher in IPF-ECFCs than in PB-ECFCs ($p = 0.015$). At 45 days, the difference was no longer significant despite a marked trend (Fig. 4a). Results were confirmed by cell-cycle analysis that revealed a cell-cycle arrest in G0-1 phase in IPF-ECFCs (Fig. 4b). Then, we quantified the level of apoptosis of IPF-ECFCs and PB-ECFCs aged 30 days. The percentage of cells in early apoptosis state (positive annexin-V cells) was significantly higher in IPF-ECFCs than in controls ($p = 0.015$) (Fig. 4c). We further assessed this difference in senescence by quantifying gene expression of three senescence regulators, *CDKN1A* (p21), *TP53* (p53), and *CDKN2A* (p16) and reported a significantly increased CDKN2A expression in IPF-ECFCs compared to controls
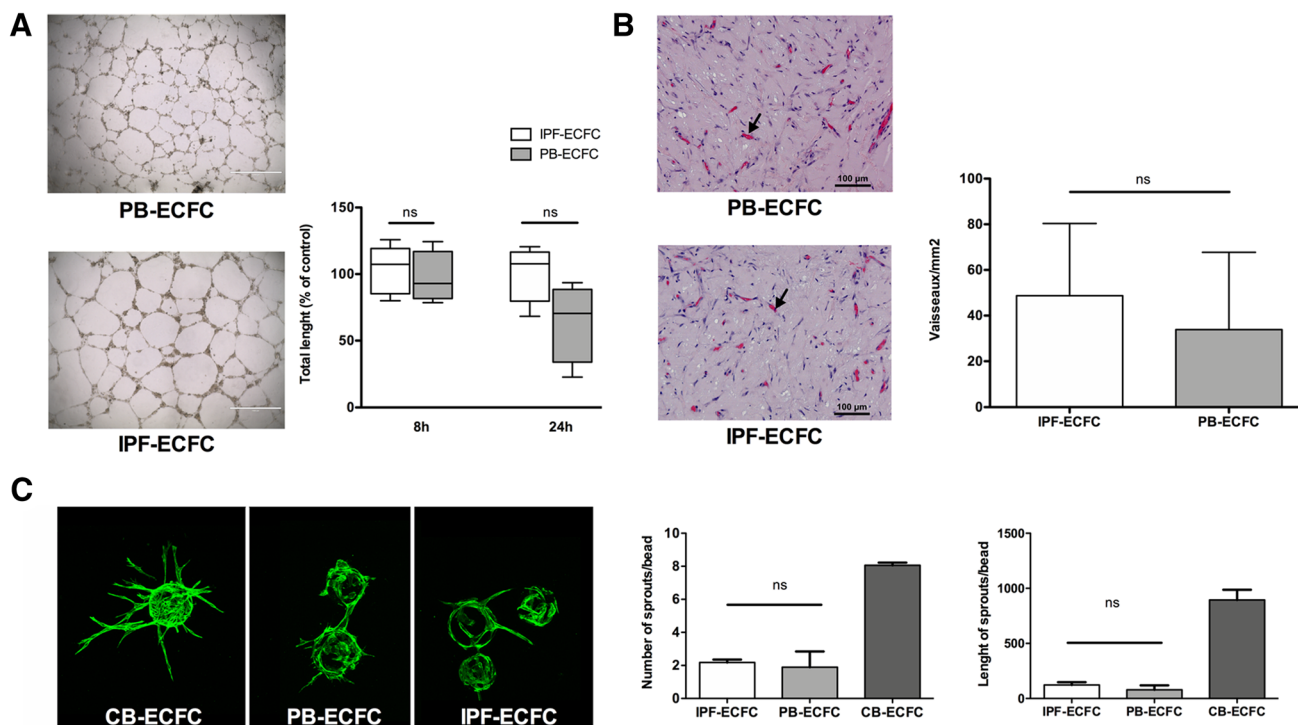
Fig. 3 Differentiation of IPF-ECFCs. **a** Formation of pseudo-tube in Matrigel™ model in vitro: images taken after 24 h (scale 1000 μm), length of tubes formed after 8 h or 24 h ($n=4$ or 5). **b** Formation of functional vessels (arrow) in a Matrigel™ model in vivo (scale 100 μm), quantification of number of vessels/mm^2 ($n=3$). **c** 3D sprouting assay, number of sprout/beads, total length of sprouts ($n=3$). ns $p > 0.05$

($p=0.04$) (Fig. 4d). Altogether, these data suggest that IPF-ECFCs are more senescent than PB-ECFCs.

IPF-ECFCs exhibit a higher IL-8 release capacity than controls

Several soluble factors secreted by ECFCs were quantified, including angiogenesis mediators (VEGF-A, FGF-2, sVEGF-R1, sVEGF-R2, HGF, G-CSF) as well as molecules related to Senescence-associated secretory phenotype (SASP) (complex pro-inflammatory response of senescent cells: IL-8, MCPs, MIPs, TGF-ββ, PAI-1, t-PA) [26]. Results presented in Table 1 show that IPF-ECFCs have a higher capacity to secrete IL-8 in vitro, compared to PB-ECFCs ($p=0.03$). This fivefold increase was only observed for IL-8 as all other angiogenesis and SASP molecules were comparable to controls. As these data are generated in a limited number of samples in a multiplex system, we replicated results in a more consistent experimental setting using ELISA, and confirmed the increased IL-8 release capacity of IPF-ECFCs compared to PB-ECFCs ($p=0.001$) (Fig. 5a). In order to determine

whether this increase was specific to IL-8 or also concerned other inflammatory mediators, IL-6 levels were assessed in conditioned medium. No difference was observed between IPF-ECFCs and PB-ECFCs (data not shown). We further tested relevance of this increased IL-8 secretion in plasma. Indeed, as shown in Fig. 5b, IL-8 concentration is significantly increased in IPF patient's plasmas compared to control plasmas ($p < 0.0001$).

IL-8 released by IPF-ECFCs induces neutrophil migration in vitro and in vivo

As IL-8 is a key mediator for neutrophil recruitment, we tested the capacity of IPF-ECFC-conditioned medium (CM) to induce neutrophil migration in a Transwell® assay. A significant increase in neutrophil migration was observed toward IPF-ECFC-CM compared to PB-ECFC-CM ($p=0.003$). Importantly, this effect was abolished by the addition of an anti-IL-8 antibody to IPF-ECFC-CM ($p=0.03$) indicating that IL-8 was largely responsible for CM chemoattractive effects (Fig. 6a). These data were further explored using a Matrigel implant assay in vivo

in which ECFCs and MSCs are known to recruit myeloid cells through a paracrine mechanism [27, 28]. We tested the effects of IPF-ECFC-CM in this model on neutrophil recruitment comparatively to PB-ECFC-CM. There was a trend toward an increased chemotactic capacity of IPF-ECFC-CM compared to PB-ECFC-CM ($p = 0.057$). The addition of an anti-IL-8 antibody in the implant significantly abolished this effect ($p = 0.03$) (Fig. 6b, c). We further tested relevance of correlation between IL-8 and PMNs in plasma. IL-8 concentration in patients' samples is correlated with their level of neutrophils ($p = 0.02$) and leucocytes ($p = 0.01$) (data not shown). As shown in Fig. 6d, patients with PMNs above 9G/L have a significant higher level of IL-8. Finally, in order to evaluate the relevance of IL-8/neutrophil mobilization in IPF lung, we performed IL-8 staining by IHC on lung sections of IPF patients and controls. We never found any positive vessels in control lungs (Supplementary Fig. 1, left panel) in contrast to IPF lung vessels (Supplementary Fig. 1, right panel). We also assessed the contribution of neutrophil infiltration to the histopathology of human IPF. There was a trend toward a more pronounced infiltration of neutrophils in IPF lungs compared to controls ($p = 0.07$) (Supplementary Fig. 2).

Increased PMNs in IPF patients are associated to a worse prognosis

We evaluated the potential prognostic value of blood neutrophil count in IPF patients in relation with the main complications of the disease (progression of IPF, acute exacerbation, development of pulmonary hypertension, requirement for lung transplantation, death). We show that in IPF subjects ($n = 65$) included into our prospective cohort, blood leukocyte and neutrophil counts at admission significantly correlated with a composite end-point regrouping the subsequent occurrence of IPF complications such acute exacerbation, disease progression, pulmonary hypertension, transplantation, or death ($p = 0.02$ and 0.01 for leukocytes and neutrophils, respectively) (Table 2).

Discussion

The mechanisms underlying the aberrant vascular remodeling process constantly observed in the IPF lung are still elusive. The endothelium compartment is known to be dysfunctional in this disease. This has been shown through local [5] as well as circulating markers of endothelial lesions [6]. Endothelial cells have been described to contribute to pulmonary fibrogenesis by promoting transition from fibroblasts to myofibroblasts [29]. In addition, we have recently shown that endothelial microvesicles isolated from IPF patients could also be involved in fibrogenesis by inducing fibroblast

migration [19]. Access to pulmonary vascular endothelial cells is tough and makes their functional evaluation difficult. ECFCs, which can be isolated from peripheral blood, may be an adequate substitute in this case. In the oncologic field, circulating tumor cells (CTC) are considered as "liquid biopsies." They are mostly used as biomarkers but it has also been shown that CTC cell lines can express cancer stem cell properties [30]. Similarly to CTCs, ECFCs might be considered as "liquid biopsies" of the endothelial compartment and represent a poorly invasive tool to explore the endothelium compartment functional properties. We previously described that ECFCs were decreased in IPF compared to healthy controls. We now hypothesized that their vasculogenic properties could be modified in IPF. For this purpose, we evaluated adhesion, migration, and differentiation capacities of ECFCs recovered from IPF patients and showed that they were similar to control PB-ECFCs. Similarly, angiogenic pathways assessed in IPF-ECFC secretome were comparable to that of PB-ECFCs.

Increased senescence has previously been shown in ECFCs from smokers and in COPD patients compared to non-smoking controls [14] but also in ECFCs from cord blood of premature babies [31]. We have shown here for the first time that a senescence profile is also found in ECFCs isolated from IPF patients. Senescence, and particularly that of alveolar epithelial cells, is now recognized as a major pathogenic pathway in IPF pathophysiology [32]. This abnormal epithelium secretes numerous mediators that trigger fibroblasts activation and lung remodeling [2]. ß-galactosidase and p16 expression were indeed increased in IPF-ECFCs as well as their early apoptosis and associated to a cell-cycle arrest. Therefore, our findings suggest accelerated aging of ECFCs in IPF patients and possibly reflect a systemic effect of lung fibrosis on circulating compartment. Interestingly, ECFCs from IPF, expanded in culture in non-oxidant conditions, retained a strong vasculogenic potential but a senescent phenotype. Endothelial senescence is a process known to increase the risk of atherosclerosis and cardiovascular disease. Therefore, one can hypothesize a participation of senescent ECFCs in the pathogenesis of cardiovascular comorbidities frequently reported during IPF [1].

In IPF-ECFCs, we found that senescence-associated secretory phenotype (SASP) was also significantly modified with a strong increase in IL-8 in the IPF-ECFC-conditioned medium. These data are in agreement with the literature in which IL-8 is demonstrated to be secreted by most senescent cell types [26] and to be associated to senescence in ECFCs [33]. However, in this paper from Medina's group, late-passage ECFCs are clearly non-responsive to IL-8 proangiogenic effects. These experiments have been conducted with CB-ECFCs. In contrary, we worked with PB-ECFCs or IPF-ECFCs that where already all senescent (even if
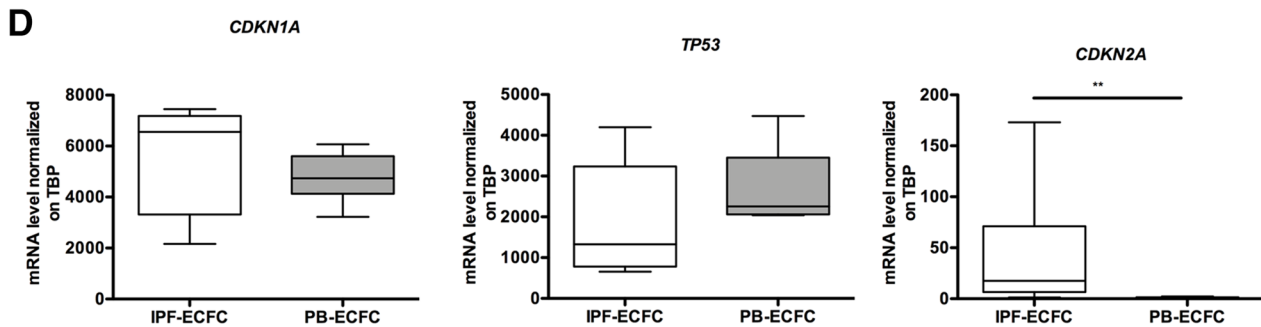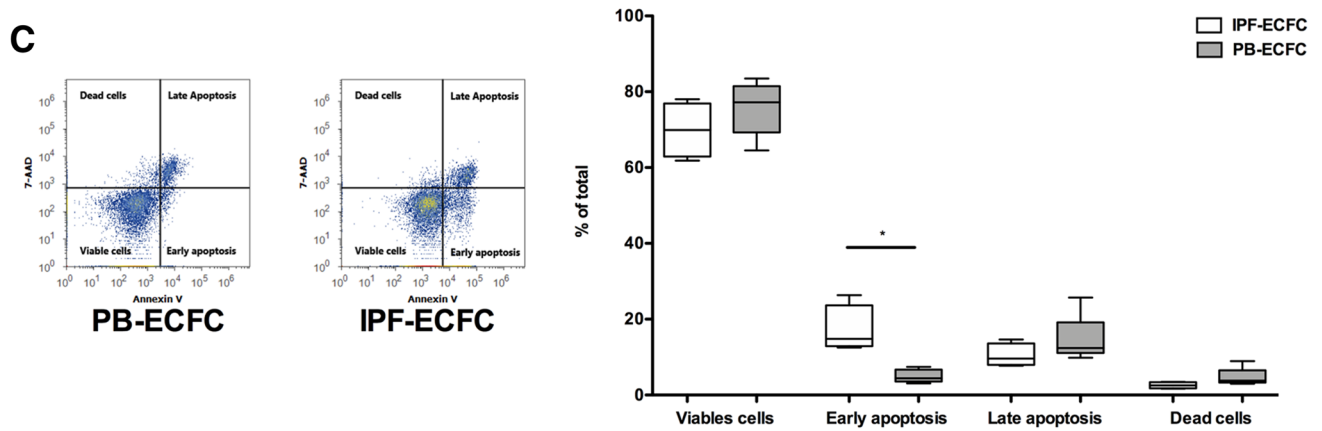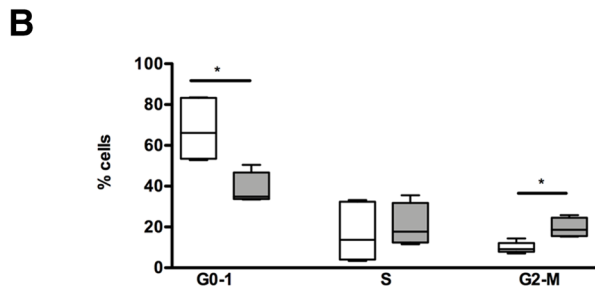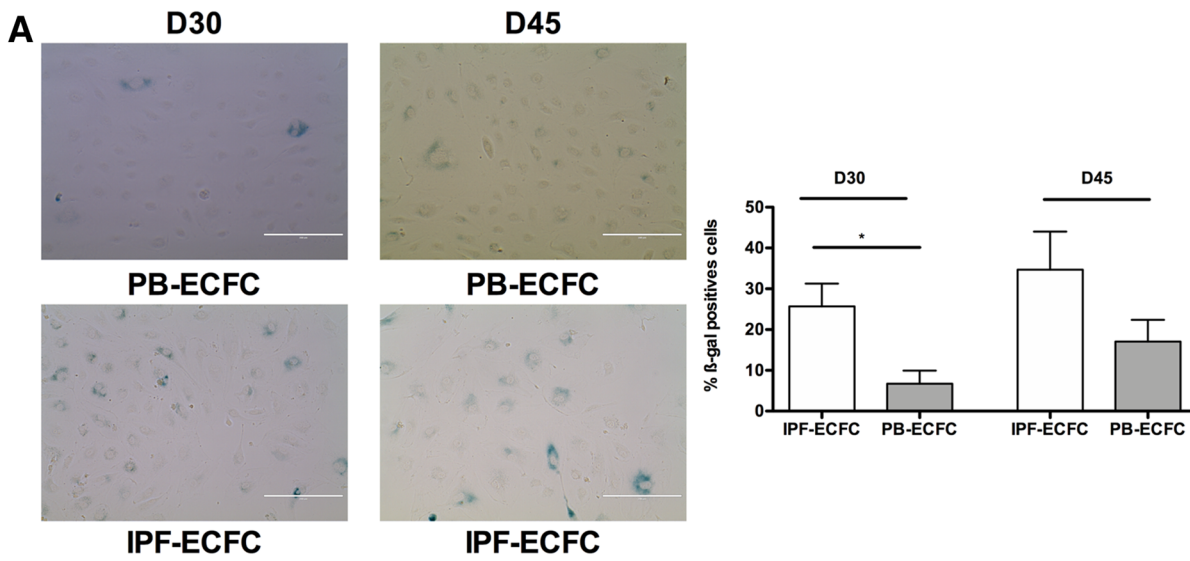
◄**Fig. 4** Evidence for senescence of IPF-ECFC. **a** β-galactosidase staining on IPF-ECFCs and PB-ECFCs, % of positive cells ($n = 3–5$). **b** Cell-cycle assessment by BrDu incorporation (% cells in G0-1, S, or G2- phase) ($n = 4–5$). **c** Apoptosis by cytometry (% of viable cells, early apoptosis, late apoptosis, or dead cells) ($n = 4–5$). **d** Quantification of gene expression of *CDKN1A, TP53*, and *CDKN2A* by RT-qPCR (n = 6). *$p < 0.05$ **$p < 0.005$

Table 1 Secretome analysis of IPF-ECFC and PB-ECFC

Soluble factor	IPF-ECFC	PB-ECFC	p
t-PA	128.1 ± 97.26	111.0 ± 76.91	ns
PAI-1	64.92 ± 31.91	40.29 ± 3.92	ns
VEGF-A	1.12 ± 2.50	0.86 ± 1.02	ns
FGF-2	5.65 ± 8.96	1.99 ± 2.46	ns
sVEGF-R1	166.2 ± 115.4	157.4 ± 209.1	ns
sVEGF-R2	91.28 ± 71.68	58.51 ± 77.23	ns
G-CSF	0.11 ± 0.261	2.46 ± 4.09	ns
HGF	17.36 ± 15.33	2.42 ± 4.08	ns
MCP-1	987.2 ± 705.0	257.4 ± 137.1	ns
IL-8	231.0 ± 118.7	44.63 ± 56.63	< 0.05
IL-6	6.73 ± 6.06	1.69 ± 2.03	ns
MIP-1α	2.31 ± 2.81	0.56 ± 0.77	ns
MIP-1β	10.59 ± 15.48	0.87 ± 1.48	ns
TGF-β1	7.16 ± 5.13	5.03 ± 3.88	ns
TNF-α	ND	ND	

Results are expressed in ng/10^6 cells

IPF-ECFCs were more senescent than PB-ECFCs) and can been considered similar as late passages cord-blood ECFCs according to Yoder's classification of endothelial colonies (HPP and LPP colonies [34]). This can explain why we did not observe any difference between IPF-ECFCs and controls in terms of angiogenic effects. Nevertheless, IL-8 effect on ECFC remains controversial. Indeed, the presence of the two IL-8 receptors CXCR1 and CXCR2 in ECFCs is not a consistent result. Their presence has been described in several papers so far [35]; however, we have never been able to demonstrate the presence of these receptors on cord-blood and adult ECFCs [36]. We repeated these results here in complete independent experiments on IPF-ECFCs and we were not able to show the presence of CXCR1 or CXCR2 in our cell by RT-qPCR (data not shown) and flow cytometry (Supplementary Fig. 3), in contrast to fibroblasts. Thus, we remain doubtful about the physiological role of IL-8 in ECFC senescence and/or proliferation. However, we clearly think that IL-8 is a consequence of ECFC senescence as a "SASP" molecule and exerts its effect of chemoattraction on PMNs or other cell types and not as an autocrine ligand of ECFCs. In 2008, we previously described that IL-8 is not secreted at basal level by ECFCs but can be expressed after an inflammatory stress like thrombin activation by PAR1-activating peptide. Thus, this IL-8 secretion after a cell stress could be in line with IL-8 secretion in case of ECFC senescence.

Several reported data strongly argue for a deregulation of IL-8 in IPF as well as for an involvement in its pathogenesis [7]. Previously described as secreted mostly by alveolar macrophages [37], fibroblasts, and alveolar cells [38], IL-8 exhibits increased levels in the bronchoalveolar lavage fluid of IPF patients, these levels being correlated with neutrophil count and disease severity [39], as well as in plasma [40] and
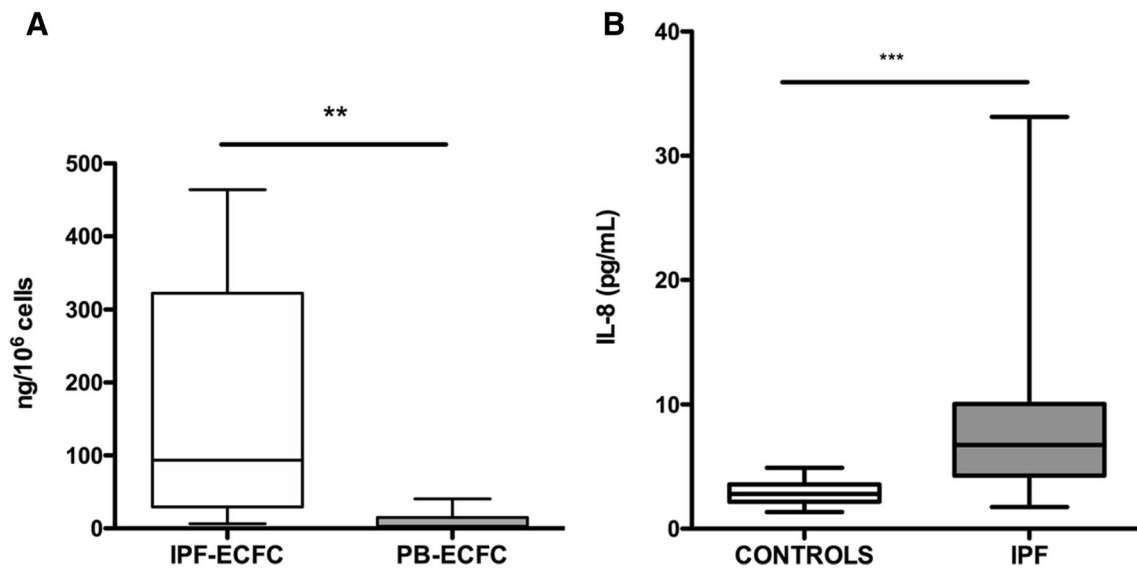
Fig. 5 IL-8 quantification in conditioned medium of IPF-ECFC and relevance in IPF patients. **a** Quantification of IL-8 in conditioned medium of IPF-ECFC ($n = 20$) and PB-ECFC ($n = 8$) by ELISA. **b** Quantification of IL-8 in IPF patients ($n = 50$) and controls healthy patients ($n = 10$) plasmas by ELISA. **$p < 0.005$ ***$p < 0.0001$

A

B

C

D
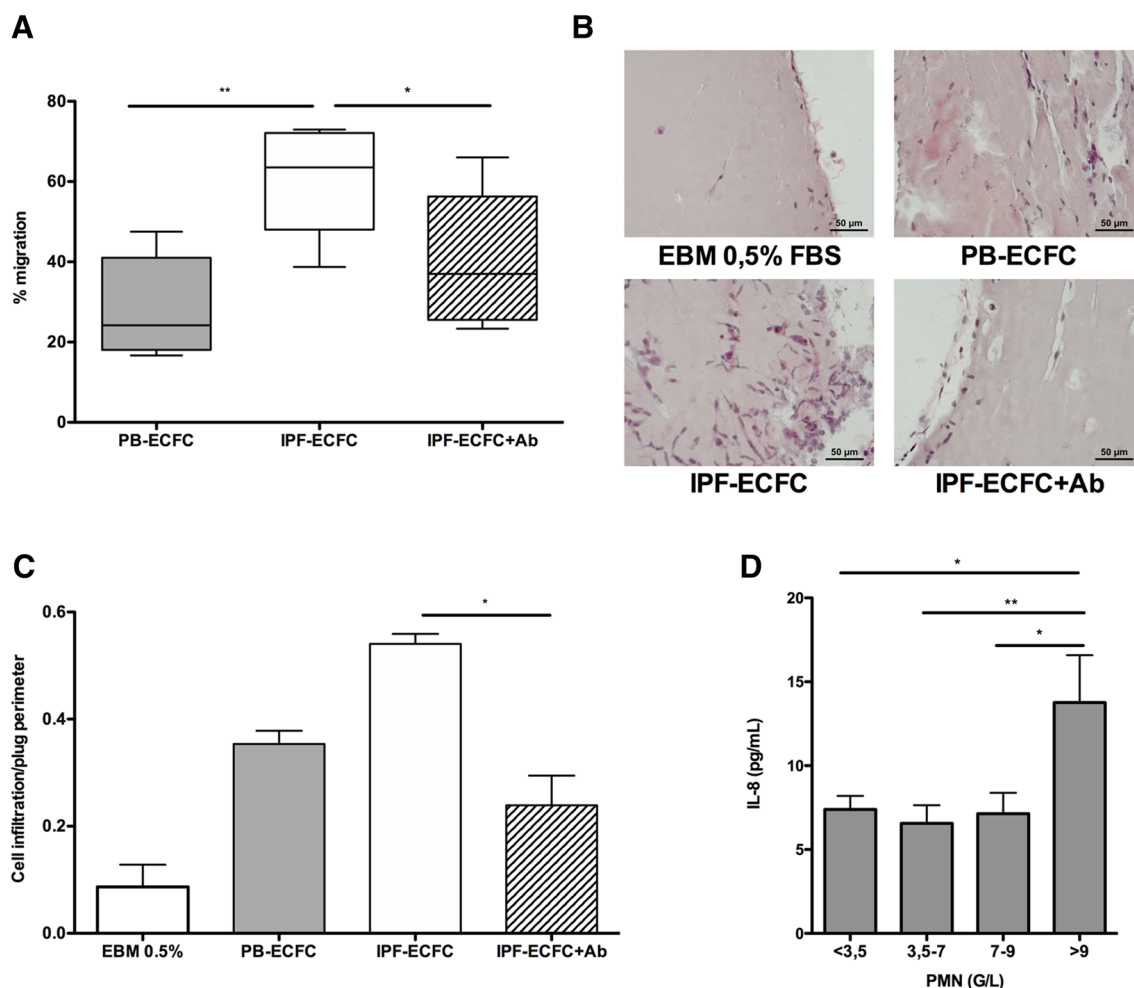
Fig. 6 Effects of IL-8 in conditioned medium of IPF-ECFCs on neutrophil migration. **a** Migration of neutrophils toward conditioned medium of PB-ECFCs ($n=5$), IPF-ECFCs ($n=10$), or IPF-ECFCs in the presence or in the absence of a IL-8 blocking antibody ($n=6$). **b** Images of plug edges for each condition (HES staining, scale 50 μm).

c Quantification of neutrophil infiltration in Matrigel implants induced by PB-ECFC-CM or IPF-ECFC-CM ($n=3$–5). **d** IL-8 concentration in IPF patients' plasma according to PMN level (<3.5 g/L, 3.5–7 g/L, 7–9 g/L or >9 g/L). *$p<0.05$ **$p<0.005$

Table 2 Hazard ratios of association between initial blood cell counts and exacerbations, suspicions of pulmonary hypertension, progression, transplantation, or death in 65 IFP patients prospectively enrolled

Blood cell counts	Hazard ratio	CI 95%	*p* value
Leukocyte count	1.15	(1.03; 1.28)	**0.015**
Neutrophil count	1.14	(1.02; 1.27)	**0.02**
Lymphocyte count	1.02	(0.68; 1.52)	0.93
Monocyte count	2.22	(0.63; 7.87)	0.22
Platelet count	1	(1; 1)	0.59
HSC (CD34+) count	1	(1; 1)	0.97

Bold values indicate significant results, $p < 0.05$

serum [41] exhibiting an association with a poor prognosis. Importantly, a minor allele of the SNP rs4073T > A in IL-8

gene promoter is associated to an increase of IL-8 expression as well as to IPF [42]. In a murine model, inhibition of MIP-2 (macrophage inflammatory protein-2), a functional homolog of IL-8, decreases bleomycin-induced pulmonary fibrosis [38]. Altogether, these data argue for an overexpression of IL-8 in the alveolar compartment of the IPF lung with a strongly suggested role in its pathogenesis and disease progression.

We showed using Boyden chambers that IPF-ECFC-CM induced an IL-8-dependent neutrophil migration. This result was confirmed in vivo using a Matrigel implant model. Matrigel implant vascularization is dependent on myeloid cell recruitment during the first days of implantation, and their recruitment is induced by paracrine secretion of cells implanted in the plug [27, 28]. In our study, inflammatory infiltrates were increased in plugs containing IPF-ECFC-CM

and largely inhibited by the concomitant use of an anti-IL-8 blocking Ab. Our study suggests a participation of IL-8 to the pulmonary infiltration by neutrophils, consistent with the observation of neutrophil infiltration in IPF lungs and neutrophil correlation with the poorest IPF prognosis at inclusion. Inflammation was once suspected to be one of the potential triggers of IPF pathophysiology but this was subsequently denied by the demonstration of a deleterious effect of immunosuppressive therapies in this disease [43]. However, a current hypothesis suggests that the recruitment and activation of immune cells can modulate the current fibrotic response of the last stages of fibrogenesis [44]. In particular, among inflammatory cells, neutrophils might play a pathogenic role as yet not elucidated. Mice deficient in neutrophil elastase (NE), a neutrophil-derived serine protease, are protected from bleomycin-induced lung fibrosis [45] and administration of NE inhibitor (sivelestat) is protective in this model [46]. In vitro, NE can induce fibroblast proliferation and differentiation [47]. Neutrophils could also be involved in the IPF pathophysiology via the regulation of metalloproteinase and in particular MMP-2, MMP-8, and MMP-9 [48]. A MMP inhibitor was indeed able to prevent bleomycin-induced pulmonary fibrosis [49]. Finally, neutrophil extracellular traps (NETs) have been implicated in fibroblast differentiation [50] further suggesting a pathogenic role of neutrophils in fibrogenesis.

In summary, our data show an up-regulation of IL-8 production by senescent ECFCs isolated from IPF patients. Blocking IL-8 impairs neutrophil migration, suggesting a mechanism for ECFC-mediated inflammatory cell migration in IPF. Increased neutrophil infiltration in IPF lung and correlation between circulating neutrophils and disease worsening in this prospective clinical cohort might be related to senescent endothelial cells. The use of ECFCs as liquid biopsy also provides a better understanding of the pathogenesis of cardiovascular disease reported in IPF patients.

Compliance with ethical standards

Conflict of interest The authors do not have any conflicts of interest to disclose.

References

1. Lederer DJ, Martinez FJ (2018) Idiopathic pulmonary fibrosis. N Engl J Med 378:1811–1823. https://doi.org/10.1056/NEJMra1705751

2. Wolters PJ, Blackwell TS, Eickelberg O et al (2018) Time for a change: is idiopathic pulmonary fibrosis still idiopathic and only fibrotic? Lancet Respir Med 6:154–160. https://doi.org/10.1016/S2213-2600(18)30007-9

3. Hashimoto N, Phan SH, Imaizumi K et al (2010) Endothelial-mesenchymal transition in bleomycin-induced pulmonary fibrosis. Am J Respir Cell Mol Biol 43:161–172. https://doi.org/10.1165/rcmb.2009-0031OC

4. Kato S, Inui N, Hakamata A et al (2018) Changes in pulmonary endothelial cell properties during bleomycin-induced pulmonary fibrosis. Respir Res 19:127. https://doi.org/10.1186/s12931-018-0831-y

5. Ebina M, Shimizukawa M, Shibata N et al (2004) Heterogeneous increase in CD34-positive alveolar capillaries in idiopathic pulmonary fibrosis. Am J Respir Crit Care Med 169:1203–1208. https://doi.org/10.1164/rccm.200308-1111OC

6. Smadja DM, Mauge L, Nunes H et al (2013) Imbalance of circulating endothelial cells and progenitors in idiopathic pulmonary fibrosis. Angiogenesis 16:147–157. https://doi.org/10.1007/s10456-012-9306-9

7. Strieter RM, Gomperts BN, Keane MP (2007) The role of CXC chemokines in pulmonary fibrosis. J Clin Invest 117:549–556. https://doi.org/10.1172/JCI30562

8. Smadja DM, Nunes H, Juvin K et al (2014) Increase in both angiogenic and angiostatic mediators in patients with idiopathic pulmonary fibrosis. Pathol Biol 62:391–394. https://doi.org/10.1016/j.patbio.2014.07.006

9. Silvestre J-S, Smadja DM, Lévy BI (2013) Postischemic revascularization: from cellular and molecular mechanisms to clinical applications. Physiol Rev 93:1743–1802. https://doi.org/10.1152/physrev.00006.2013

10. d'Audigier C, Susen S, Blandinieres A et al (2018) Egfl7 represses the vasculogenic potential of human endothelial progenitor cells. Stem Cell Rev Rep 14:82–91. https://doi.org/10.1007/s12015-017-9775-8

11. Basile DP, Yoder MC (2014) Circulating and tissue resident endothelial progenitor cells. J Cell Physiol 229:10–16. https://doi.org/10.1002/jcp.24423

12. Toshner M, Voswinckel R, Southwood M et al (2009) Evidence of dysfunction of endothelial progenitors in pulmonary arterial hypertension. Am J Respir Crit Care Med 180:780–787. https://doi.org/10.1164/rccm.200810-1662OC

13. Baker CD, Balasubramaniam V, Mourani PM et al (2012) Cord blood angiogenic progenitor cells are decreased in bronchopulmonary dysplasia. Eur Respir J 40:1516–1522. https://doi.org/10.1183/09031936.00017312

14. Paschalaki KE, Starke RD, Hu Y et al (2013) Dysfunction of endothelial progenitor cells from smokers and chronic obstructive pulmonary disease patients due to increased DNA damage and senescence. Stem Cells Dayt Ohio 31:2813–2826. https://doi.org/10.1002/stem.1488

15. Fadini GP, Schiavon M, Rea F et al (2007) Depletion of endothelial progenitor cells may link pulmonary fibrosis and pulmonary hypertension. Am J Respir Crit Care Med 176:724–725. https://doi.org/10.1164/ajrccm.176.7.724a author reply 725.

16. Díez M, Musri MM, Ferrer E et al (2010) Endothelial progenitor cells undergo an endothelial-to-mesenchymal transition-like process mediated by TGFbetaRI. Cardiovasc Res 88:502–511. https://doi.org/10.1093/cvr/cvq236

17. Raghu G, Collard HR, Egan JJ et al (2011) An official ATS/ERS/JRS/ALAT statement: idiopathic pulmonary fibrosis: evidence-based guidelines for diagnosis and management. Am J Respir Crit Care Med 183:788–824. https://doi.org/10.1164/rccm.2009-040GL

18. Mauge L, Sabatier F, Boutouyrie P et al (2014) Forearm ischemia decreases endothelial colony-forming cell angiogenic potential. Cytotherapy 16:213–224. https://doi.org/10.1016/j.jcyt.2013.09.007

19. Bacha NC, Blandinieres A, Rossi E et al (2018) Endothelial Microparticles are Associated to Pathogenesis of Idiopathic Pulmonary Fibrosis. Stem Cell Rev 14:223–235. https://doi.org/10.1007/s12015-017-9778-5

20. Arnulf B, Lecourt S, Soulier J et al (2007) Phenotypic and functional characterization of bone marrow mesenchymal stem cells derived from patients with multiple myeloma. Leukemia 21:158–163. https://doi.org/10.1038/sj.leu.2404466

21. Smadja DM, Bièche I, Helley D et al (2007) Increased VEGFR2 expression during human late endothelial progenitor cells expansion enhances in vitro angiogenesis with up-regulation of integrin alpha(6). J Cell Mol Med 11:1149–1161. https://doi.org/10.1111/j.1582-4934.2007.00090.x

22. Nakatsu MN, Sainson RCA, Aoto JN et al (2003) Angiogenic sprouting and capillary lumen formation modeled by human umbilical vein endothelial cells (HUVEC) in fibrin gels: the role of fibroblasts and Angiopoietin-1. Microvasc Res 66:102–112

23. Eglinger J, Karsjens H, Lammert E (2017) Quantitative assessment of angiogenesis and pericyte coverage in human cell-derived vascular sprouts. Inflamm Regen 37:2. https://doi.org/10.1186/s41232-016-0033-2

24. Smadja D, Gaussem P, Roncal C et al (2010) Arterial and venous thrombosis is associated with different angiogenic cytokine patterns in patients with antiphospholipid syndrome. Lupus 19:837–843. https://doi.org/10.1177/0961203309360985

25. Ferratge S, Ha G, Carpentier G et al (2017) Initial clonogenic potential of human endothelial progenitor cells is predictive of their further properties and establishes a functional hierarchy related to immaturity. Stem Cell Res 21:148–159. https://doi.org/10.1016/j.scr.2017.04.009

26. Coppé J-P, Desprez P-Y, Krtolica A, Campisi J (2010) The senescence-associated secretory phenotype: the dark side of tumor suppression. Annu Rev Pathol 5:99–118. https://doi.org/10.1146/annurev-pathol-121808-102144

27. Melero-Martin JM, De Obaldia ME, Allen P et al (2010) Host myeloid cells are necessary for creating bioengineered human vascular networks in vivo. Tissue Eng Part A 16:2457–2466. https://doi.org/10.1089/ten.TEA.2010.0024

28. Lin R-Z, Lee CN, Moreno-Luna R et al (2017) Host non-inflammatory neutrophils mediate the engraftment of bioengineered vascular networks. Nat Biomed Eng 1: 0081. https://doi.org/10.1038/s41551-017-0081

29. Yin Q, Nan H-Y, Zhang W-H et al (2011) Pulmonary microvascular endothelial cells from bleomycin-induced rats promote the transformation and collagen synthesis of fibroblasts. J Cell Physiol 226:2091–2102. https://doi.org/10.1002/jcp.22545

30. Pantel K, Alix-Panabières C (2016) Functional studies on viable circulating tumor cells. Clin Chem 62:328–334. https://doi.org/10.1373/clinchem.2015.242537

31. Vassallo PF, Simoncini S, Ligi I et al (2014) Accelerated senescence of cord blood endothelial progenitor cells in premature neonates is driven by SIRT1 decreased expression. Blood 123:2116–2126. https://doi.org/10.1182/blood-2013-02-484956

32. Selman M, Pardo A (2014) Revealing the pathogenic and aging-related mechanisms of the enigmatic idiopathic pulmonary fibrosis. An integral model. Am J Respir Crit Care Med 189:1161–1172. https://doi.org/10.1164/rccm.201312-2221PP

33. Medina RJ, O'Neill CL, O'Doherty TM et al (2013) Ex vivo expansion of human outgrowth endothelial cells leads to IL-8-mediated replicative senescence and impaired Vasoreparative function: IL8 mediates OEC senescence. STEM CELLS 31:1657–1668. https://doi.org/10.1002/stem.1414

34. Ingram DA (2004) Identification of a novel hierarchy of endothelial progenitor cells using human peripheral and umbilical cord blood. Blood 104:2752–2760. https://doi.org/10.1182/blood-2004-04-1396

35. Kimura T, Kohno H, Matsuoka Y et al (2011) CXCL8 enhances the angiogenic activity of umbilical cord blood-derived outgrowth endothelial cells in vitro. Cell Biol Int 35:201–208. https://doi.org/10.1042/CBI20090225

36. Smadja DM, Bièche I, Susen S et al (2009) Interleukin 8 is differently expressed and modulated by PAR-1 activation in early and late endothelial progenitor cells. J Cell Mol Med 13:2534–2546. https://doi.org/10.1111/j.1582-4934.2008.00429.x

37. Carré PC, Mortenson RL, King TE et al (1991) Increased expression of the interleukin-8 gene by alveolar macrophages in idiopathic pulmonary fibrosis. A potential mechanism for the recruitment and activation of neutrophils in lung fibrosis. J Clin Invest 88:1802–1810. https://doi.org/10.1172/JCI115501

38. Keane MP, Belperio JA, Moore TA et al (1999) Neutralization of the CXC chemokine, macrophage inflammatory protein-2, attenuates bleomycin-induced pulmonary fibrosis. J Immunol 1950 162:5511–5518

39. Richter AG, Perkins GD, Chavda A et al (2011) Neutrophil chemotaxis in granulomatosis with polyangiitis (Wegener's) and idiopathic pulmonary fibrosis. Eur Respir J 38:1081–1088. https://doi.org/10.1183/09031936.00161910

40. Richards TJ, Kaminski N, Baribaud F et al (2012) Peripheral blood proteins predict mortality in idiopathic pulmonary fibrosis. Am J Respir Crit Care Med 185:67–76. https://doi.org/10.1164/rccm.201101-0058OC

41. Fujimori Y, Kataoka M, Tada S et al (2003) The role of Interleukin-8 in interstitial pneumonia. Respirology 8:33–40

42. Ahn M-H, Park B-L, Lee S-H et al (2011) A promoter SNP rs4073T> A in the common allele of the interleukin 8 gene is associated with the development of idiopathic pulmonary fibrosis via the IL-8 protein enhancing mode. Respir Res 12:73

43. Raghu G, Rochwerg B, Zhang Y et al (2015) An official ATS/ERS/JRS/alat clinical practice guideline: treatment of idiopathic pulmonary fibrosis. An update of the 2011 clinical practice guideline. Am J Respir Crit Care Med 192:e3–e19. https://doi.org/10.1164/rccm.201506-1063ST

44. Desai O, Winkler J, Minasyan M, Herzog EL (2018) The role of immune and inflammatory cells in idiopathic pulmonary fibrosis. Front Med 5:. https://doi.org/10.3389/fmed.2018.00043

45. Chua F, Dunsmore SE, Clingen PH et al (2007) Mice lacking neutrophil elastase are resistant to bleomycin-induced pulmonary fibrosis. Am J Pathol 170:65–74. https://doi.org/10.2353/ajpath.2007.060352

46. Takemasa A, Ishii Y, Fukuda T (2012) A neutrophil elastase inhibitor prevents bleomycin-induced pulmonary fibrosis in mice. Eur Respir J 40:1475–1482. https://doi.org/10.1183/09031936.00127011

47. Gregory AD, Kliment CR, Metz HE et al (2015) Neutrophil elastase promotes myofibroblast differentiation in lung fibrosis. J Leukoc Biol 98:143–152. https://doi.org/10.1189/jlb.3HI1014-493R

48. Henry MT, McMahon K, Mackarel AJ et al (2002) Matrix metalloproteinases and tissue inhibitor of metalloproteinase-1 in sarcoidosis and IPF. Eur Respir J 20:1220–1227

49. Corbel M, Caulet-Maugendre S, Germain N et al (2001) Inhibition of bleomycin-induced pulmonary fibrosis in mice by the matrix

metalloproteinase inhibitor batimastat. J Pathol 193:538–545. https://doi.org/10.1002/path.826

50. Chrysanthopoulou A, Mitroulis I, Apostolidou E et al (2014) Neutrophil extracellular traps promote differentiation and function of fibroblasts. J Pathol 233:294–307. https://doi.org/10.1002/path.4359